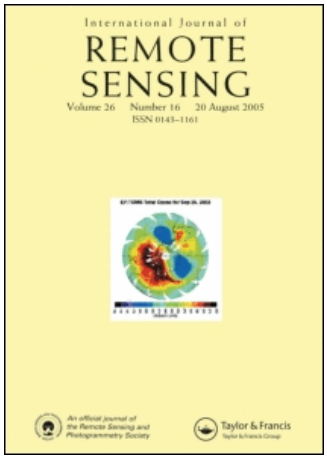

International Journal of Remote Sensing
Publication details, including instructions for authors and subscription information:
http://www.informaworld.com/smpp/title~content=t713722504

Multispectral images fusion by a joint multidirectional and multiresolution representation

Online Publication Date: 01 January 2007
To cite this Article: Lillo-Saavedra, M. and Gonzalo, C. (2007) 'Multispectral images fusion by a joint multidirectional and multiresolution representation', International Journal of Remote Sensing, 28:18, 4065 - 4079
To link to this article: DOI: 10.1080/01431160601105884
URL: http://dx.doi.org/10.1080/01431160601105884

International Journal of Remote Sensing
Vol. 28, No. 18, 20 September 2007, 4065–4079

Multispectral images fusion by a joint multidirectional and multiresolution representation

M. LILLO-SAAVEDRA*† and C. GONZALO‡
†Faculty of Agricultural Engineering, University of Concepción, Av. Vicente Méndez 595, Casilla 537 Chillán, Chile
‡School of Computer Science, Department of Architecture and Technology of Computers, Technical University of Madrid, Campus Montegancedo, Boadilla del Monte, 28660 Madrid, Spain

(*Received 19 January 2006; in final form 2 November 2006*)

This paper proposes a new fusion method that permits an adequate selection of information extracted from source images to obtain fused images with good spatial and spectral quality simultaneously. This method is based on a joint multiresolution multidirectional representation of the source images using a single directional spatial frequency low pass filter bank of low computational complexity, defined in the Fourier domain. The source images correspond to those captured by the IKONOS satellite (panchromatic and multispectral). The results obtained indicate that the proposed method provides, in a simple manner, objective control over the trade-off between high spatial and spectral quality of the fused images.

1. Introduction

Image fusion can be understood as the synergetic combination of information provided from several sensors, or by the same sensor in different scenarios (e.g. spatial, spectral and temporal). From a multispectral (MULTI) and panchromatic (PAN) image fusion perspective, which will be discussed in this paper, image fusion consists of combining the spectral information of the MULTI image with the spatial information of the PAN image in a coherent manner. To improve the quality of the fused images, researchers have sought to find new image representations.

In the last decade, the most commonly used image fusion strategies were based on multiresolution analysis techniques. Their objective was to find a discrete transform that minimizes the intrinsic uncertainty associated with the joint representation of information. From this point of view, the Discrete Wavelet Transform (DWT) can be considered as the most popular approximation (e.g. Garguet-Duport *et al.* 1996, Yocky 1996).

Despite the good results provided by the DWT in the image fusion field, there are several aspects that have yet to be resolved. One aspect is the precise selection of the details, extracted from the PAN image, minimizing the quantity of spectral information that this contributes to the fused image, and preserving the spectral quality of the MULTI image. Another aspect is the control of the inherent trade-off between the spatial and spectral quality of the fused image. Indeed, it can be

*Corresponding author. Email: malillo@udec.cl

International Journal of Remote Sensing
ISSN 0143-1161 print/ISSN 1366-5901 online
http://www.tandf.co.uk/journals
DOI: 10.1080/01431160601105884

confirmed that the multiresolution transforms with low anisotropy are not capable of intrinsically controlling this trade-off.

In this sense, different approximations have been proposed, for example, Garzelli *et al.* (2004), Lillo-Saavedra and Gonzalo (2006) and Yunhao *et al.* (2006). All of them weight the quantity of the information from the PAN image that is integrated into the degraded MULTI image, using different strategies in order to find a trade-off between the spatial and spectral quality of the fused images.

In this context, a new highly anisotropic and redundant fusion method that provides an adequate selection of information extracted from the source images is required. The present paper responds to this need with a proposal for a new fusion method, which includes both aspects, which is based on a joint multiresolution and multidirectional representation of images to be fused, using a single directional filter bank of low computational complexity, defined in the Fourier domain.

The present work is structured into six sections. Section 2 presents a series of ideas and concepts on the processing and fusion of images, this forms the base of the multidirectional and multiresolution representation proposed in §3. In §4, the new fusion method is developed. The results obtained are presented and discussed in §5. And finally, §6 presents the most relevant conclusions.

2. Background

The DWT is a linear transformation that is very useful in signal processing. One of its principal applications consists of separating datasets into distinct frequency components, which are then represented on common scales. It should be noted that the multidimensional versions of this transform are built from one-dimensional (1-D) bases. Therefore, the two-dimensional (2-D) version is capable of detecting discontinuities from single points, but does not favour their integration into continuous segments. Consequently, this 2-D transform cannot efficiently detect smooth discontinuities (Do and Vetterli 2001). This is one of the reasons that justified the search for new image representations, defined by bases that match their dimensionality.

There are different ways of calculating the Wavelet transform, among which the most important is the pyramidal algorithm of Mallat (Pohl and van Garderen 1998, Zhou *et al.* 1998, Mallat 1999, Ranchin and Wald 2000). The Mallat transform is one of the most widely used due to its high spectral quality of the resulting image. However, its low anisotropic nature still produces some problems for the fusion of images with a high content of borders that are not horizontal, vertical or diagonal (Candès and Donoho 2000). Dutilleux (1987) has proposed a Wavelet *à trous* (with holes) algorithm. This algorithm differs from the pyramidal ones in that it presents an isotropic nature and is redundant, which implies that between two consecutive degradation levels, there is no dyadic spatial compression of the original image, but rather the size of the image is maintained. Several works have shown that redundant Wavelet transforms provide better results in determined image processing applications such as noise elimination (Malfait and Roose 1997), texture classification (Unser 1995), and, more recently, in the case of image fusion (Nuñez *et al.* 1999, Chibani and Houacine 2003).

The recent appearance of new transforms, such as Curvelets (Candès and Donoho 1999a), Ridgelets (Candès and Donoho 1999b) and Contourlets (Do and Vetterli 2005), which are more efficient than the DWT from the information representation perspective, opens a new field of research in the image fusion algorithm area. These

new transforms are highly anisotropic and produce a much more efficient extraction of spatial details in different directions. In particular, the characteristics of the Contourlet Transform (CT) provide the bases of the fusion method proposed in this paper.

2.1 *Contourlet transform*

In contrast with other transforms that were initially defined in a continuous domain and then applied in a discrete domain, the CT was originally defined in a discrete domain, with the utilization of a filter bank structure, and then it was generalized in a continuous domain using a multiresolution analysis method (Do and Vetterli 2005). Additionally, the capacity of this transform to capture the intrinsic geometric structure of the images resides in its authentic 2-D nature, in contrast with other transforms that can be defined as separable extensions of 1-D transforms.

The concept that is behind the CT implies a multiresolution transform that detects borders, followed by a local and directional transform that detects contour segments present in the image. For their implementation, Do and Vetterli (2005) proposed a structure defined by a double filter bank, the Laplacian Pyramidal (LP) transform (Starck *et al.* 1998) to capture isolated points and a directional filter bank to join these points in linear structures. In this manner, the CT can be considered as a base of functions of ellipsoidal (elongated) support with different scales, directions and aspect relations.

The final structure of this double filter bank corresponds to a pyramidal directional filter bank (PDFB) (Do and Vetterli 2001). This structure is displayed graphically in figure 1. The application of the double filter bank can be observed in the figure. Moreover, it is important to realize, that the number of directions is doubled by going to the next scale in the pyramid. This is done to satisfy the anisotropy scaling relation (width $\propto$ length^2) as described in Do and Vetterli (2001).

The CT is not spatially invariant due to the downsampler and upsampler operators implied in its calculations (Do and Vetterli 2005). Cunha *et al.* (2005) proposed a redundant version of this transform, substituting the LP transform for the *à trous* algorithm. This new transform reduces the complexity of the design of the filters to a multiresolution filter bank and a directional filter bank.

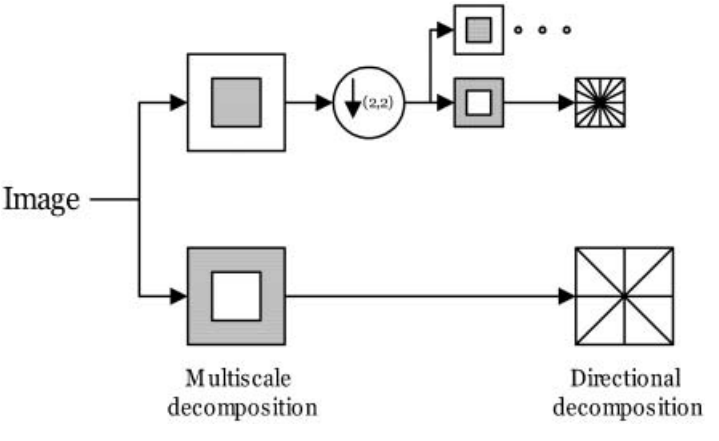

Figure 1. A flow graph of the contourlet transform. The image is first decomposed into different frequency sub-bands by the Laplacian pyramid transform and then the high frequency sub-band image is decomposed by a directional filter bank.

2.2 *Directional filter bank*

Despite the need in many image processing areas for filters that simultaneously present great directional sensitivity and maximum decimation, most research has treated these aspects separately. Bamberger and Smith (1992) proposed a 2-D directional filter bank (DFB) that combined both aspects. This DFB extracts the directional components, with a minimum number of samples equal to the components of the original image, and from which an exact reconstruction of the image is possible. The implementation of this DFB is based on a structure of levels, with two channels for each level. Each level is implemented using separable filters. After this, numerous studies were performed in order to improve the loans, efficiency and applications of this type of DFB (Bamberger 1993, Park *et al.* 1999, Hong and Smith 2002, Park *et al.* 2004). All these approximations maintain the concept of decimation, which, for several applications, is not always desirable. In addition, even when the difficulties associated with the filter design have been reduced (Nguyen and Oraintara 2005), this task maintains a certain conceptual and computational complexity. These limitations have been overcome by a new approximation proposed by Lakshmanan (2004). In this approach, the DFB presents non separable behaviour, and consequently it maintains the characteristics of this filter type, but is implemented as a sum of two separable filters, notably diminishing the calculation requirements. The following section describes this DFB implementation.

3. A new joint multidirectional and multiresolution representation for analysis and synthesis of images

The new joint representation proposed in this work is based on a single directional low pass filter bank. This transform seeks to combine the simplicity of the Wavelet transform, calculated using the *à trous* algorithm (TWA), with the benefits of multidirectional transforms like the CT.

In general, the majority of the multiresolution and multidirectional image representations are based on the application of a double filter bank. One filter bank is for stepping from a higher to a lower resolution level. The second filter bank is directional and it allows the directional characteristics in each one of the levels to be captured. The present study utilizes a single directional low pass filter bank (DLPFB) that joins the two tasks. Thus, at each level (θ_n), where n is the level, image degradation is performed applying a low pass filter with a determined orientation, in the Fourier domain computed by the fast Fourier transform (FFT):

$$\mathrm{Image}_{\theta_n}(x, y) = \mathrm{FFT}^{-1}\left\{\mathrm{FFT}\left[\mathrm{Image}_{\theta_{n-1}}(x, y)\right] H_{\theta_n}(u, v)\right\}, \tag{1}$$

where θ_{n-1} is the degradation level prior to the transform application, and $H_{\theta_n}(u, v)$ represents the directional low pass filter transfer function applied at level θ_n. The directional information is extracted by finding the differences of the directional degraded images on two consecutive levels, and is stored in the transform's coefficients associated with each level:

$$\mathrm{Coef}_{\theta_n}(x, y) = \mathrm{Image}_{\theta_n}(x, y) - \mathrm{Image}_{\theta_{n-1}}(x, y). \tag{2}$$

Figure 2 graphically illustrates the realization of this transform.

From equations (1) and (2), the original image can be exactly reconstructed by using equation (3):

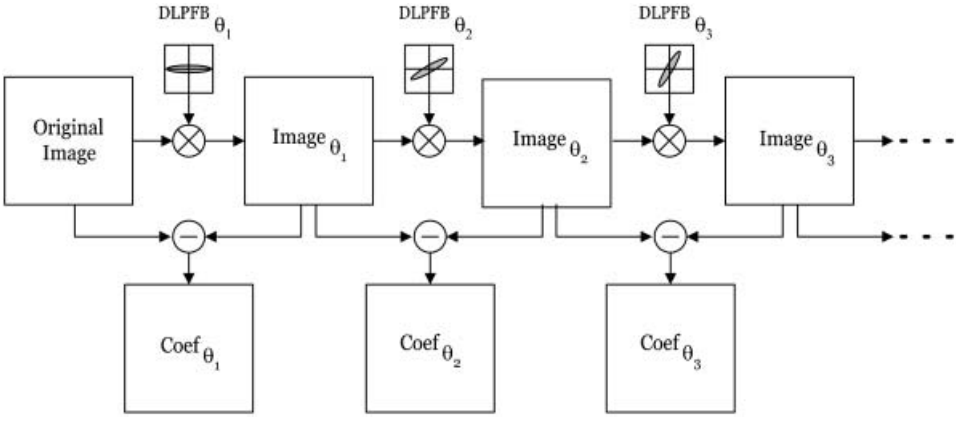

Figure 2. Flow diagram of the proposed joint multiresolution and multidirectional images representation.

$$\text{Image}(x, y) = \text{Image}_{\theta_k}(x, y) + \sum_{n=1}^{k} \text{Coef}_{\theta_n}(x, y). \tag{3}$$

In other words, it adds all the directional coefficients (Coef_{θ_n}) to the corresponding image at the higher degradation level (θ_k), in a procedure analogous to the one used in the TWA.

3.1 *Directional filter design*

Lakshmanan (2004) demonstrated that a low pass filter $H(u,v)$ that was simultaneously separable and directional could not exist. However, a directional low pass filter that was defined as the sum of two separable filters was possible. In particular, if one considers the following transfer function ($H(u,v)$) for an ellipsoidal filter whose orientation is determined by the angle θ:

$$H(u, v) = \begin{cases} 1 & \text{if } \dfrac{(u\cos\theta - v\sin\theta)^2}{a^2} + \dfrac{(u\sin\theta - v\cos\theta)^2}{b^2} \le 1 \\ 0 & \text{otherwise} \end{cases}. \tag{4}$$

The parameters a and b are defined as the filter scale and its elongation respectively. Under these conditions, Lakshmanan (2004) demonstrated that it has an approximate form:

$$H(u, v) = H_1(u) \times H_2(v) - \alpha u H_1(u) \times v H_2(v), \tag{5}$$

where α is given by the relation $(a^2–b^2)\sin(2\theta;)/(a^2b^2)$ and:

$$H_1(u) = \exp\left(-u^2 \left(\frac{\cos^2\theta}{a^2} + \frac{\sin^2\theta}{b^2} \right) \right), \tag{6}$$

$$H_2(u) = \exp\left(-v^2 \left(\frac{\cos^2\theta}{b^2} + \frac{\sin^2\theta}{a^2} \right) \right). \tag{7}$$

The most interesting characteristic of this filter is not its elliptic form, but rather its directional character by which it assigns high weights to the corresponding values in a determined direction and low weights to their orthogonal direction.

The construction of a DLPFB to obtain the transform of a given image requires setting the values of a and b, and assigning k values to the angle θ. A DLPFB of this type divides the frequency space into k portions, capturing the image's directional characteristics. Figure 3 presents the kernels of the low pass filters defined in the Fourier domain for three different directions (0°, 45° and 90°).

It is important to note that the values of a and b determine the geometry of the low pass filters that conform to the DLPFB. From an image representation perspective, the values that these parameters take will determine the quantity of image information contained in the coefficients, and in each one of the degraded images. In the case being studied here, this quality of image information determines the final quality of the fused image, as will be shown in the following section.

4. Fusion method

Similar to other fusion methods for MULTI and PAN images, the objective of the proposed method is to integrate coherently the low frequency information from the MULTI image and the high frequency information from the PAN image, in order to obtain a fused image whose spatial quality would be as similar as possible to the quality of a high resolution spatial image (PAN), whilst still conserving the spectral characteristics of a high resolution spectral image (MULTI).

Under the previous considerations, this paper proposes a new image fusion method that is formally expressed in equation (8):

$$\mathrm{FUS}^{\mathrm{i}}(x, y) = \mathrm{MULTI}^{\mathrm{i}}_{\theta_k}(x, y) + \sum_{\mathrm{n}=1}^{\mathrm{k}} \mathrm{Coef}^{\mathrm{PAN}}_{\theta_n}(x, y), \tag{8}$$

where $\mathrm{FUS}^{\mathrm{i}}(\mathrm{x,y})$ represents the i^{th} band of the fused image, $\mathrm{MULTI}^{\mathrm{i}}_{\theta_k}(\mathrm{x}, \mathrm{y})$ represents the i^{th} band of the MULTI image degraded in k directions, and $\mathrm{Coef}^{\mathrm{PAN}}_{\theta_n}(\mathrm{x}, \mathrm{y})$ represents the PAN image coefficients from equation (2).

The two most relevant characteristics of this method are its high anisotropy, and the control of the inherent compromise between spatial and spectral quality of the fused image. As indicated earlier, the parameters a and b determine the filter geometry and, consequently, the information selected in the filtering process. One of the objectives of the present study is to determine the quality dependence of the

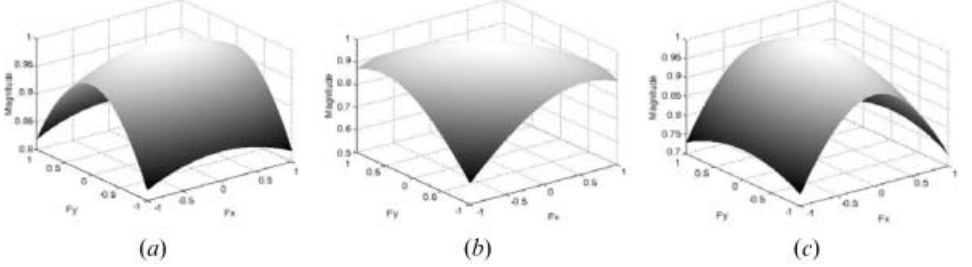

Figure 3. Kernels of the filters defined in the Fourier domain for θ equal to: (*a*) 0°, (*b*) 45°, and (*c*) 90°.

fused images on the a and b parameters, and the number of frequency partitioning (k) used for image decomposition. A sensitivity analysis of the spatial and spectral quality of the fused images against these parameters has been performed. The indices used to evaluate these qualities have been the spectral ERGAS (Wald 2002) and spatial ERGAS (Lillo-Saavedra *et al.* 2005) indices.

The definition of spectral ERGAS (*Erreur Relative Globale Adimensionalle de Synthèse*) (Wald 2002) is given by equation (9):

$$\mathrm{ERGAS}_{\mathrm{spectral}} = 100\frac{\mathrm{h}}{\mathrm{l}}\sqrt{\frac{1}{N_{\mathrm{Bands}}}\sum_{\mathrm{i}=1}^{N_{\mathrm{Bands}}}\left(\frac{\left(\mathrm{RMSE}_{\mathrm{spectral}}\left(\mathrm{Band}^{\mathrm{i}}\right)\right)^2}{\left(\mathrm{MULTI}^{\mathrm{i}}\right)^2}\right)}, \tag{9}$$

where h and l represent the spatial resolution of the PAN and MULTI images respectively; N_{Bands} is the number of bands of the fused image; $\mathrm{MULTI}^{\mathrm{i}}$ is the radiance value of the i^{th} band of the MULTI image and $\mathrm{RMSE}_{\mathrm{spectral}}$ is defined as:

$$\mathrm{RMSE}_{\mathrm{spectral}}\left(\mathrm{Band}^{\mathrm{i}}\right) = \frac{1}{\mathrm{NP}}\sqrt{\sum_{\mathrm{j}=1}^{\mathrm{NP}}\left(\mathrm{MULTI}^{\mathrm{i}}(\mathrm{j}) - \mathrm{FUS}^{\mathrm{i}}(\mathrm{j})\right)^2}, \tag{10}$$

where NP is the number of pixels of the fused image and $\mathrm{FUS}^{\mathrm{i}}$ represents the i^{th} band of the fused image.

Given that, in the definition of the spectral ERGAS index (equation (9)), only spectral characteristics of the source images to be fused were considered, Lillo-Saavedra *et al.* (2005) proposed a new index with the objective of evaluating the spatial quality of these images. This new index is inspired in the spectral ERGAS and has been named the spatial ERGAS:

$$\mathrm{ERGAS}_{\mathrm{spatial}} = 100\frac{\mathrm{h}}{\mathrm{l}}\sqrt{\frac{1}{N_{\mathrm{Bands}}}\sum_{\mathrm{i}=1}^{N_{\mathrm{Bands}}}\left(\frac{\left(\mathrm{RMSE}_{\mathrm{spatial}}\left(\mathrm{Band}^{\mathrm{i}}\right)\right)^2}{\left(\mathrm{PAN}^{\mathrm{i}}\right)^2}\right)}, \tag{11}$$

where $\mathrm{PAN}^{\mathrm{i}}$ is the image obtained by adjusting the histogram of the original PAN image to the histogram of the i^{th} band of the MULTI image. And finally, $\mathrm{RMSE}_{\mathrm{spatial}}$ has been defined as:

$$\mathrm{RMSE}_{\mathrm{spatial}}\left(\mathrm{Band}^{\mathrm{i}}\right) = \frac{1}{\mathrm{NP}}\sqrt{\sum_{\mathrm{j}=1}^{\mathrm{NP}}\left(\mathrm{PAN}^{\mathrm{i}}(\mathrm{j}) - \mathrm{FUS}^{\mathrm{i}}(\mathrm{j})\right)^2}. \tag{12}$$

Two main reasons have suggested the use of these indices to carry out the cited sensitivity analysis. The first reason is that since both indices have a common domain of variation (see equations (9) and (12)), their comparison is feasible. The second reason is the great sensitivity of the ERGAS indices with respect to the degradation level that characterizes the multi-resolution fusion methods (Gonzalo and Lillo-Saavedra 2004).

Since it is well known that the spectral quality decreases with the degradation level while spatial quality increases, the goal is to study how spatial and spectral resolutions vary for different values of the parameters a and b for each degradation level or frequency partitioning. The study performed here has demonstrated the

intrinsic capacity of the proposed method to control both spatial and spectral quality of the fused images.

5. Experimental results and discussion

The data used to evaluate this method corresponds to a 1600 m^2 scene of images recorded on 10 March 2000 by panchromatic (PAN) and multispectral (MULTI) sensors of the IKONOS satellite. Geographically, the scene is located in the Maipo Valley, near to Santiago city, Chile. The ratio between the spatial resolution of the PAN image (1m) and the MULTI (4m) image is 1 : 4. In order to achieve a correct integration of the data coming from both source images, it was first necessary to georeference the MULTI and PAN images, and then resample the MULTI images to the size of the PAN images.

A colour composition of near infrared (N), green (G), and blue (B) bands of the original MULTI image is presented in figure 4(*a*), and the corresponding PAN image is shown in figure 4(*b*).

For this study, a scene was selected where the predominant coverage was either vegetable or urban, with a large quantity of lines that defined the different estates, as well as streets and roads, which allow the evaluation of the highly directional (anisotropic) characteristic of the proposed fusion algorithm.

As mentioned in §3.1, the values of the filter parameters a and b determine the geometry of the low pass filter to be used. A ratio between these two parameters close to 1 generates circular filters, while values far from 1 generate elliptical filters. To carry out the sensitivity study mentioned above, a large quantity of experiments were performed, obtaining fused images for different frequency partitioning ($k=2^1$, 2^2, 2^3, 2^4, 2^5, 2^6 and 2^7) and for different combinations of a and b.

In a first analysis, the values of the filter parameters (a and b) are segmented into two intervals. The first is defined between 0.1 and 0.5 with steps of 0.1, while the second one is defined between 1 and 5 with steps of 1. In this way, the combinations are considered to be 100 for each set of frequency partitioning (k). Subsequently, the

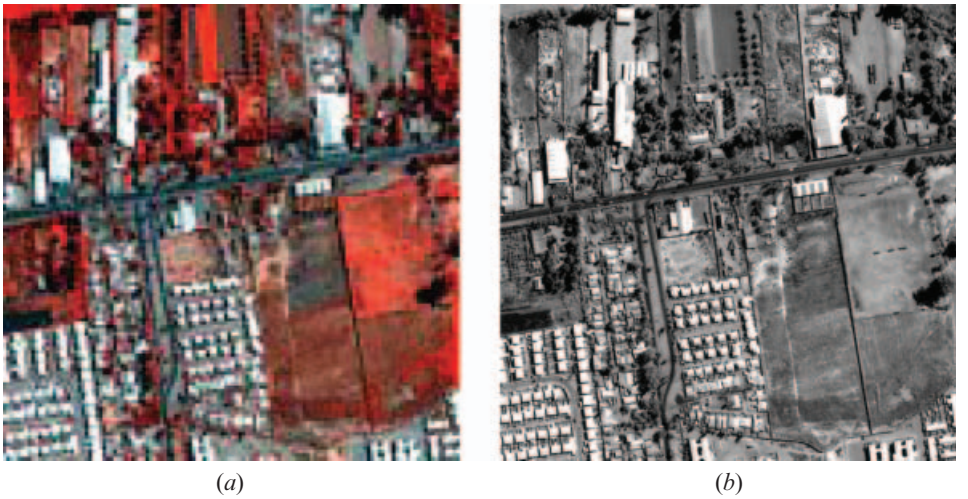

(*a*) (*b*)

Figure 4. Source images: (*a*) NGB composition of the MULTI image, and (*b*) PAN image.

spatial and spectral quality, as well as their average and standard deviation values were evaluated using the ERGAS indices.

The analysis of these results indicated that, for the particular cases of k equal to 2^1 and 2^7, the fused images with better global quality were obtained when the ratio between a and b was close to 1. This implies circular filters with a low or null directionality, providing images of very low spatial quality in the first case ($k=2^1$), since the number of directions in which the frequency space has been divided is very low. The second case ($k=2^7$) has low spectral quality due to an excessive number of directional degradations of the original MULTI image.

For the remaining space partitions, quite regular performances were observed. Sustained growth in both parameters (a and b) worsens spatial quality and increases spectral quality of the fused image. This result confirms the inverse compromise that exists between both qualities of the fused image, mentioned by Lillo-Saavedra *et al.* (2005). These aspects are displayed in figure 5, where the surfaces of the spatial, spectral, and average ERGAS indices are represented for the fused image with $k=2^3$ directions.

In figure 5, it can be observed that great symmetry exists with respect to the plane diagonal defined by the parameters a and b, which proves the expected highly symmetric behaviour of these parameters. Additionally, it can be appreciated how the compromise between spatial and spectral quality of the fused image can be controlled by varying the DLPFB parameters. Another aspect that can be observed in figure 5 is the existence of an intersection zone between the surfaces of the spatial and spectral ERGAS indices, with a low value for the average ERGAS index and a standard deviation close to 0 ($\sigma \approx 0$). These zones correspond to the filters that provide the best compromise between both qualities.

The results obtained also show that, for each one of the frequency partitioning, there is a set of values of the filter parameters for which the compromise between spatial and spectral quality is better. A unique value of b has been determined for a range of values of a (a_{min} to a_{max}) in which the lower average ERGAS values are

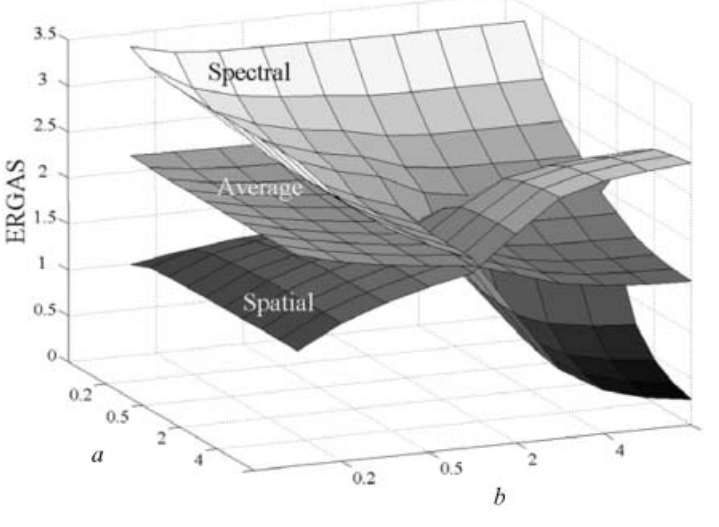

Figure 5. Surfaces of the spatial and spectral ERGAS indices and their average values of fused images ($k=2^3$).

Table 1. ERGAS spatial and spectral values, their averages and standard deviations for the images fused with a_{min}.

Filter parameters			ERGAS			
Freq. partitioning (k)	a_{min}	b	Spatial	Spectral	Average	Std. dev.(σ)
2^2	1	0.5	1.9887	1.8678	1.9283	0.0855
2^3	2	0.6	1.9750	1.8947	1.9348	0.0568
2^4	2	0.8	1.9418	1.9508	1.9463	0.0063
2^5	1	1.0	1.7492	2.3128	2.0310	0.1553

obtained. In particular, for this study, fused images with their ERGAS values (both spatial and spectral) less than or very close to 2 were only considered.

Tables 1 and 2 show the values of the filter design parameters for a_{min} and a_{max} respectively. These provided the best compromises between spatial and spectral quality. Also shown are the values corresponding to the spatial and spectral ERGAS indices, their averages, and standard deviations (σ).

For k equal to 2^2 and 2^5, the variation range of parameter a is between 1 and 5, and for parameter b, the range is between 0.5 and 1 respectively. For k equal to 2^3 and 2^4, the variation range of the parameter a is restricted between 2 and 5, with values of b equal to 0.6 and 0.8 respectively.

As can be appreciated from tables 1 and 2, better ERGAS spatial values are obtained when a larger number of orientations in the frequency spaces are considered. However, this results in a deterioration of spectral quality, since it assumes a larger number of degradations of the MULTI image. Analysing the average ERGAS values, it can be observed that the lowest corresponds to $k=2^2$, while the best compromise ($\sigma \approx 0$) is for $k=2^4$. In this sense, it can be considered that the best equilibrium for the average and standard ERGAS values is obtained for $k=2^3$. The best set of values to fuse the image considered in this study is $k=2^3$, $a=5$ and $b=0.6$.

Figure 6(*a*) presents a MULTI image degraded in 2^3 directions, using the filter bank designed with the parameters indicated in table 2. Additionally, figure 6 presents the coefficients of the PAN image associated with the particular directions (*b*) 0°, (*c*) 30°, (*d*) 45°, (*e*) 60°, and (*f*) 90°. In these figures, the directionality of the details of each one can be observed.

Figure 7(*a*) displays the NGB composition of the fused image using the method proposed here with the parameter set that provides the best trade-off between the spatial and spectral quality. A visual analysis indicates a noteworthy increase in

Table 2. ERGAS spatial and spectral values, their averages and standard deviations for the images fused with a_{max}.

Filter parameters			ERGAS			
Freq. partitioning (*k*)	a_{max}	b	Spatial	Spectral	Average	Std. dev.(σ)
2^2	5	0.5	2.0326	1.7975	1.9151	0.1662
2^3	5	0.6	1.9738	1.8966	1.9352	0.0546
2^4	5	0.8	1.9575	1.9240	1.9408	0.0237
2^5	5	1.0	1.9001	2.0257	1.9629	0.0888

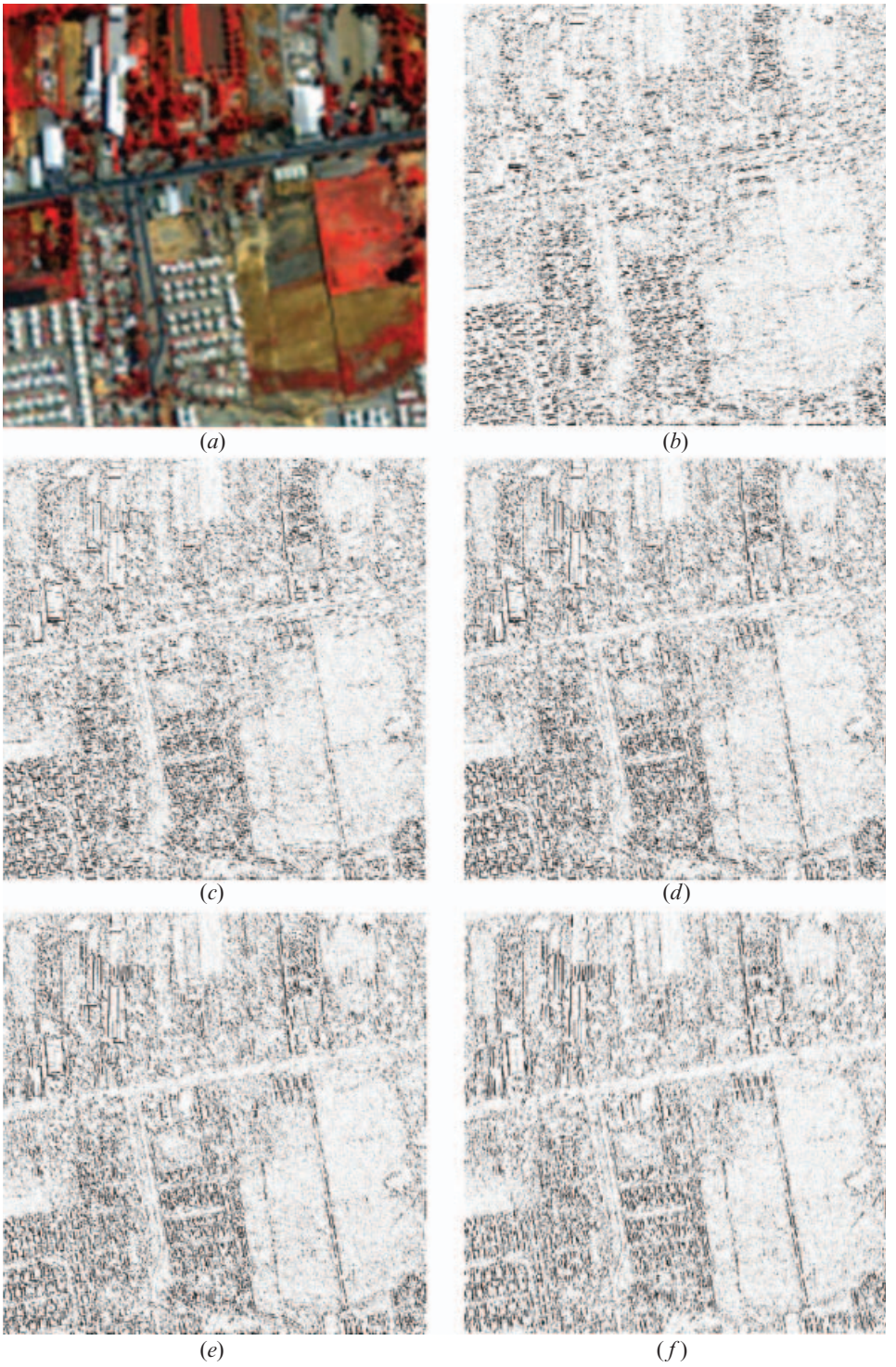

Figure 6. For k=2^3, a=5 and b=0.6: (*a*) NGB composition of the degraded MULTI image, and PAN image coefficients for: (*b*) θ=0°, (*c*) θ=30°, (*d*) θ=45°, (*e*) θ=60°, and (*f*) θ=90°.

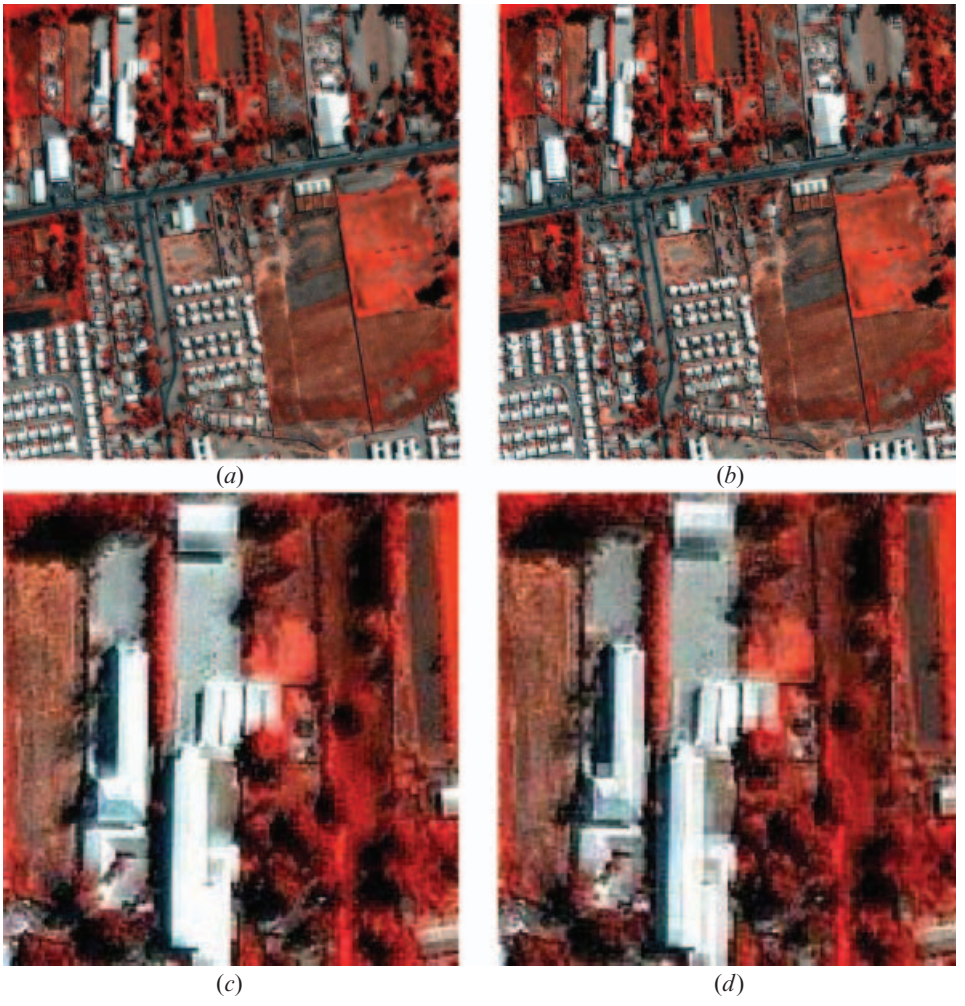

Figure 7. NGB composition of the fused images: (*a*) method proposed here ($k=2^3$, $a=5$ and $b=0.6$), (*b*) Wavelet Mallat method, (*c*) zoomed image obtained using proposed method, and (*d*) zoomed image obtained using Wavelet Mallat algorithm.

spatial quality with respect to the original image (figure 4(*a*)), whilst still maintaining the spectral quality, as shown in the colour conservation.

In order to compare the performances of the new method against other methods, the Wavelet transform, calculated by the Mallat algorithm has been selected, due to its extensive use elsewhere. Figure 7(*b*) shows an image fused using this method. The ERGAS values obtained for this image are $ERGAS_{spectral}=2.1079$ and $ERGAS_{spacial}=2.0801$, both of which are higher than the corresponding values obtained for the images shown in figure 7(*a*). On the other hand, and with the aim to carry out a visual comparison between both results, zooms of the two images have been included in figures 7(*c*) and (*d*). It can be observed in these two last images that the transitions in high gradient zones are much smoother for the fused image obtained through the method proposed here than for the Mallat method. This implies that the proposed method does not produce the saw-tooth phenomenon in the lines with orientation distinct from the horizontal, vertical and diagonal lines

(González-Audicana *et al.* 2005), which ratifies the highly and controlled anisotropic character of the transform using this fusion method.

6. Conclusions

This study has proposed a new multispectral image fusion method based on a joint multiresolution and multidirectional representation. This representation has been implemented through a single directional low pass filter bank (DLPFB).

One advantage of this representation is its simplicity in comparison to other similar ones that use several filter banks. Additionally, the DLPFB used is reduced to the sum of separable filters; consequently, its computational complexity is quite low.

Furthermore, the proposed fusion method is highly anisotropic due to the multi-directional characteristics of the new images representation used. Consequently, it has the capacity to preserve image spatial characteristics in every orientation.

To research the influence of the filter bank characteristics on the quality of the fused images, a study was performed for a representative range of the parameters a and b for different frequency partitioning. As a general conclusion, the results suggest that this method has the intrinsic capacity to control the global quality (spatial and spectral) of the fused images. This control is based on an adequate frequency partitioning, as well as on the selection of the a and b values.

Therefore, it has been observed that when the frequency partitioning varies between 2^2 and 2^6, fused images with better global quality are obtained. Additionally, for each frequency partitioning, there is a value of the parameter b and a range of values of the parameter a (a_{min} to a_{max}) for which fused images with high spatial and spectral quality are simultaneously obtained, with the average ERGAS values being less than 2 in the majority of the cases. For the scene considered in this study, the fused image with the most equilibrated spatial and spectral characteristics ($ERGAS_{average}=1.9352$ and $\sigma=0.0546$) has been obtained for $k=2^3$, $a=5$ and $b=0.6$.

Acknowledgments

The work presented in this paper has been jointly supported by the AECI (Spain) and the University of Concepción (Chile) (D/2214/04 and DIUC 204.131.007-1.0).

The authors gratefully acknowledge the financial support given by the Chilean Research Council (FONDECYT 11060056) and AECI (Spain).

References

BAMBERGER, R.H., 1993, New results on two and three dimensional directional filter banks. In *Proceedings of 27th Asilomar Conference Signals, Systems, Computers*, **2**, pp. 1286–1290.

BAMBERGER, R.H. and SMITH, M.J.T., 1992, A filter bank for the directional decomposition of image: theory and design. *Transactions on Signal Processing*, **40**, pp. 882–893.

CANDÈS, E.J. and DONOHO, D.L., 1999a, Curvelets: a surprisingly effective nonadaptive representation for objects with edges. In *Curve and Surfaces, L. Schumaker, et al.* (Eds) (Nashville, TN: Vanderbilt University Press).

CANDÈS, E.J. and DONOHO, D.L., 1999b, Ridgelets: the key to higher-dimensional intermittency? *Philosophical Transactions of the Royal Society, London, A*, **357**, pp. 2495–2509.

CANDÈS, E.J. and DONOHO, D.L., 2000, Curvelets, multiresolution representation, and scaling laws. In *Proceedings of SPIE Wavelet Applications in Signal and Image Processing VIII*, A. Aldroubi, A. Laine and M. Unser (Eds), 4119, pp. 1–12.

CHIBANI, Y. and HOUACINE, A., 2003, Redundant versus orthogonal wavelet decomposition for multisensor image fusion. *Pattern Recognition*, **36**, pp. 879–887.

CUNHA, A., ZHOU, J. and DO, M., 2005, Nonsubsampled contourlet transform: filter design and applications in Denoising. In *IEEE International Conferences on Image Processing*, **1**, pp. 749–752.

DO, M. and VETTERLI, M., 2001, Pyramidal directional filters bank and curvelets. In *IEEE International Conferences on Image Processing*, **3**, pp. 158–161.

DO, M. and VETTERLI, M., 2005, The contourlet transform: an efficient directional multiresolution image representation. *IEEE Transactions on Image Processing*, **14**, pp. 2091–2106.

DUTILLEUX, P., 1987, An implementation of the algorithm à trous to compute the wavelet transform. *Compt-rendus du congrès ondelettes et méthodes temps-fréquence et espace des phases*, J. Combes, A. Grossmann and Ph. Tchanitchian (Eds), pp. 298–304 (Marseille: Springer-Verlag).

GARGUET-DUPORT, B., GIREL, J., CHASSERY, J. and PAUTOU, G., 1996, The use of multiresolution analysis and wavelets transform for merging SPOT panchromatic and multispectral image data. *Photogrammetric Engineering and Remote Sensing*, **62**, pp. 1057–1066.

GARZELLI, A., NENCINI, F. and ALPARONE, L., 2004, Pan-sharpening of multispectral images: a critical review and comparison. In *Proceedings of IEEE International Geoscience and Remote Sensing Symposium*, pp. 81–84.

GONZÁLEZ-AUDICANA, M., OTAZU, X., FORS, O. and SECO, A., 2005, Comparison between the Mallat's and the *à trous* discrete wavelet transform based algorithms for the fusion of multispectral and panchromatic images. *International Journal of Remote Sensing*, **26**, pp. 597–616.

GONZALO, C. and LILLO-SAAVEDRA, M., 2004, Customized fusion of satellite images based on a new *à trous* algorithm. In *Proceedings of SPIEE Conference, Image and Signal Processing for Remote Sensing*, X.L. Bruzzone (Ed.) Bellingham, WA, **5573**, pp. 444–451.

HONG, P. and SMITH, M.J., 2002, An octave-band family of nonredundant directional filterbanks. In *Proceedings of International Conference of Acoustic, Speech, Speech and Signal Processing*, pp. 1165–1168.

LAKSHMANAN, V., 2004, A separable filter for directional smoothing. *IEEE Geoscience and Remote Sensing Letters*, **1**, pp. 192–195.

LILLO-SAAVEDRA, M. and GONZALO, C., 2006, Spectral or spatial quality for fused satellite imagery? A trade-off solution using wavelet à trous algorithm. *International Journal of Remote Sensing*, **27**, pp. 1453–1464.

LILLO-SAAVEDRA, M., GONZALO, C., ARQUERO, A. and MARTINEZ, E., 2005, Fusion of multispectral and panchromatic satellite sensor imagery based on tailored filtering in the Fourier domain. *International Journal of Remote Sensing*, **26**, pp. 1263–1268.

MALFAIT, M. and ROOSE, D., 1997, Wavelet-based image denoising using a Markov random field a priori model. *IEEE Transactions on Image Processing*, **6**, pp. 549–565.

MALLAT, S., 1999, *A Wavelet Tour of Signal Processing*, Second edition (Elsevier Academic Press).

NGUYEN, T. and ORAINTARA, S., 2005, Multiresolution direction filterbanks: theory, design, and applications. *IEEE Transactions on Signal Processing*, **53**, pp. 3895–3905.

NÚÑEZ, J., OTAZU, X., FORS, O., PRADES, A., PALÁ, V. and ARBIOL, R., 1999, Multiresolution-based image fusion with additive wavelet decomposition. *IEEE Transactions on Geoscience and Remote Sensing*, **37**, pp. 1204–1211.

PARK, S.I., SMITH, M.J. and MERSEREAU, R.M., 1999, A new directional filterbank for image analysis and classification. In *Proceedings of IEEE International Conference of Acoustic, Speech and Signal Processing*, pp. 1417–1420.

PARK, S.I., SMITH, M.J. and MERSEREAU, R.M., 2004, Improved structures of maximally decimated directional filter banks for spatial image analysis. *IEEE Transactions on Image Processing*, **13**, pp. 1424–1431.

POHL, C. and VAN GENDEREN, J.L., 1998, Multisensor Image Fusion in Remote Sensing: Concepts, Methods and Application. *International Journal of Remote Sensing*, **19**, pp. 823–854.

RANCHIN, T. and WALD, L., 2000, Fusion of high spatial and spectral resolution image: the ARSIS concept and its implementation. *Photogrammetric Engineering and Remote Sensing*, **66**, pp. 49–61.

STARCK, J.L., MURTAGH, F. and BIJAOUI, A., 1998, *Image Processing and Data Analysis. The Multiscale Approach* (Cambridge: Cambridge University Press).

UNSER, M., 1995, Texture classification and segmentation using wavelet frames. *IEEE Transactions on Image Processing*, **4**, pp. 1549–1560.

WALD, L., 2002, *Data Fusion, Definition and Architectures: Fusion of Image of Different Spatial Resolution* (Paris: Le Presses de l'École des Mines).

YOCKY, D.A., 1996, Multiresolution wavelet decomposition image merger of landsat thematic mapper and spot panchromatic data. *Photogrammetric Engineering and Remote Sening*, **62**, pp. 1067–1074.

YUNHAO, C., LEI, D., JING, L., XIAOBING, L. and PEIJUN, S., 2006, A new wavelet-based image fusion method for remotely sensed data. *International Journal of Remote Sensing*, **27**, pp. 1465–1476.

ZHOU, J., CIVCO, D.L. and SILANDER, J.A., 1998, A wavelet method to merge Landsat TM and SPOT panchromatic data. *International Journal of Remote Sensing*, **19**, pp. 743–757.